Exact Thermalization Dynamics in the "Rule 54" Quantum Cellular Automaton

Katja Klobas,[1] Bruno Bertini,[1] and Lorenzo Piroli[2, 3]

[1]*Rudolf Peierls Centre for Theoretical Physics, Clarendon Laboratory,*
Oxford University, Parks Road, Oxford OX1 3PU, United Kingdom
[2]*Max-Planck-Institut für Quantenoptik, Hans-Kopfermann-Str. 1, 85748 Garching, Germany*
[3]*Munich Center for Quantum Science and Technology, Schellingstraße 4, 80799 München, Germany*

We study the out-of-equilibrium dynamics of the quantum cellular automaton known as "Rule 54". For a class of low-entangled initial states, we provide an analytic description of the effect of the global evolution on finite subsystems in terms of simple quantum channels, which gives access to the full thermalization dynamics at the microscopic level. As an example, we provide analytic formulae for the evolution of local observables and Rényi entropies. We show that, in contrast to other known examples of exactly solvable quantum circuits, Rule 54 does not behave as a simple Markovian bath on its own parts, and displays typical non-equilibrium features of interacting integrable many-body quantum systems such as finite relaxation rate and interaction-induced dressing effects. Our study provides a rare example where the full thermalization dynamics can be solved exactly at the microscopic level.

When a generic isolated quantum many-body system is driven out of equilibrium, its local properties are eventually described by the thermal ensemble. This picture can be intuitively explained by saying that, in the thermodynamic limit, the system acts as a bath for its own local sub-systems [1–5]. In light of the undeniable success of this paradigm, it is perhaps surprising that for interacting systems most of the evidence in its support comes from numerical computations in relatively small systems. The reason is that computing the full many-body relaxation dynamics in the presence of interactions poses formidable challenges that are difficult to overcome even in "exactly solvable" systems like quantum integrable models [5–7].

Recently, a useful arena to construct tractable models of many-body physics out of equilibrium has been identified in *quantum circuits*. In the simplest setting, one considers a one-dimensional ($1D$) set of qudits evolved by a "brickwork" circuit, where a given initial state is updated by sequences of local unitary gates (cf. Fig. 1). While in general quantum circuits offer no simplification with respect to local-Hamiltonian dynamics [8], the discreteness of the evolution makes it possible to construct non-trivial solvable models, with notable examples given by random [9–12] and dual unitary circuits [13]. These systems proved to be useful minimal models for the quantum chaotic dynamics, enabling the analysis of aspects that are notoriously hard to tackle in traditional systems [9–37]. However, when seen as models for thermalization, they are not typical: for instance, in dual-unitary circuits the action of the global evolution on any subsystem is purely Markovian, even in the absence of noise [14, 19, 38].

In this Letter, we present an exact solution for the thermalization dynamics in a quantum circuit that provably exhibits typical features of interacting many-body systems: the quantum version of the "Rule 54" cellular automaton [39]. The latter can be regarded as the simplest interacting integrable system and over the last years has been shown to provide an ideal ground for studying interacting many-body dynamics [40–53].
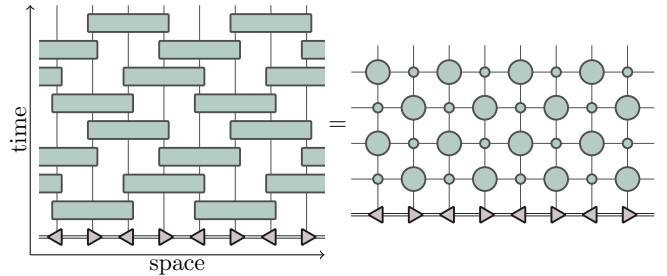

FIG. 1. Quantum circuit representation of the Rule 54 QCA. The dynamics can be equivalently given in terms of three-site gates (left) and as an MPO (right).

Our approach is based on a general tensor network (TN) algorithm introduced in Ref. [54, 55] (see also [56]) to describe the evolution of any subsystem in the thermodynamic limit. Specifically, we identify a set of algebraic relations obeyed by the tensors of Rule 54 that enable us to follow such an algorithm analytically. We use this to derive exact formulae for the evolution of local observables, two-point correlation functions and Rényi entropies, providing a rare example where the full microscopic dynamics can be solved exactly, beyond non-interacting models and the perfectly Markovian regime.

Rule 54 is defined by a $1D$ lattice of qubits where the time evolution is discrete and generated by the unitary operator $\mathbb{U} = \mathbb{U}_e \mathbb{U}_o$, with $\mathbb{U}_e = \prod_j U_{2j-1,2j,2j+1}$, $\mathbb{U}_o = \prod_j U_{2j,2j+1,2j+2}$. In the local computational basis $\{|s_j\rangle_j\}_{s_j=0,1}$, the matrix elements of the three-site unitary gate $U_{j-1,j,j+1}$ read

$$U^{s'_1 s'_2 s'_3}_{s_1 s_2 s_3} = \delta_{s_1,s'_1} \delta_{\chi(s_1,s_2,s_3),s'_2} \delta_{s_3,s'_3}, \tag{1}$$

where $\chi(s_1, s_2, s_3) \equiv (s_1 + s_2 + s_3 + s_1 s_3) \bmod 2$. Note that this update rule causes a non-zero scattering shift for quasiparticles [39]. The operators $U_{j-1,j,j+1}$ and $U_{j+1,j+2,j+3}$ commute, which allows us to write $\mathbb{U}$ in the form of a brickwork quantum circuit (Fig. 1). We

consider periodic chains of length $2L$, eventually taking $L \to \infty$.

We study a quench protocol [57, 58] where the system is initialised in a low-entangled state, which we take to be a matrix product state (MPS) [59, 60] $|\Psi_0\rangle = \sum_{i_1,\dots,i_{2L}=0,1} \mathrm{tr}\left(A_1^{i_1} \dots A_{2L}^{i_{2L}}\right)|i_1,\dots,i_{2L}\rangle$, where A_j are $\mathcal{D}$-dimensional matrices ($\mathcal{D}$ is called the bond dimension).

It is straightforward to see that $\mathbb{U}_e$, $\mathbb{U}_o$ can be represented as two-site shift invariant matrix product operators (MPO) with $\mathcal{D} = 2$ [61], so that the evolution can be computed by applying a sequence of MPOs to $|\Psi(0)\rangle$. Note that this representation is completely general, since any quantum cellular automata can be expressed exactly as an MPO with finite bond-dimension [62–64].

The expectation value of a local observable $\langle\Psi(t)|\mathcal{O}_x|\Psi(t)\rangle$ evolving via MPOs is naturally represented by the TN depicted in Fig. 2. In fact, it is convenient to think of such an object in the so-called *folded* representation [54], where the original TN is bent in half so that each tensor associated with $U^\dagger$ ends up lying on top of the corresponding tensor of U. This procedure yields a new TN generated by a *folded transfer matrix* $\mathbb{W}$, where the dimensions of local and auxiliary degrees of freedom are squared. These steps are depicted in Fig. 2, where $\mathbf{?} = \begin{bmatrix} 1 & 0 & 0 & 1 \end{bmatrix}$, represents the folded identity operator and the dynamics are defined by the folded tensors

$$
\begin{aligned}
s_1 r_1 \!-\!\!\overset{s_4 r_4}{\underset{s_2 r_2}{\bigcirc}}\!\!-\! s_3 r_3 &= \delta_{\chi(s_1,s_2,s_3),s_4}\,\delta_{\chi(r_1,r_4,r_3),r_2}, \\[2mm]
s_1 r_1 \!-\!\!\overset{s_4 r_4}{\underset{s_2 r_2}{\bigcirc}}\!\!-\! s_3 r_3 &= \prod_{j=1}^{3}\delta_{s_j,s_{j+1}}\delta_{r_j,r_{j+1}}.
\end{aligned}
\tag{2}
$$

At this point, following Refs. [54, 55], it is instructive to look at the expectation value in the *t-channel*. Namely, to view the diagram in Fig. 2 as the TN formed by the product of $2L$ MPOs acting on the lattice in time and propagating in space (a similar t-channel description has found useful applications also in the study of spectral properties [65–68]). Specifically we have

$$
\langle\Psi(t)|\mathcal{O}_x|\Psi(t)\rangle = \mathrm{tr}\left[\tilde{\mathbb{W}}^{L-1}\tilde{\mathbb{W}}[\mathcal{O}_x]\right].
\tag{3}
$$

Here, we denoted by $\tilde{\mathbb{W}}$ the MPO encoding the evolution along the "space direction", while $\tilde{\mathbb{W}}[\mathcal{O}_x]$ corresponds to the transfer matrix associated with the application of the single-site operator $\mathcal{O}_x$, cf. Fig. 2. It is straightforward to show that $\tilde{\mathbb{W}}$ has a unique largest eigenvalue $\bar{\lambda} = 1$ [61]. Exploiting this fact, we can evaluate Eq. (3) in the thermodynamic limit, obtaining

$$
\lim_{L\to\infty}\langle\Psi(t)|\mathcal{O}_x|\Psi(t)\rangle = \langle L|\tilde{\mathbb{W}}[\mathcal{O}_x]|R\rangle,
\tag{4}
$$

where $\langle L|$ and $|R\rangle$ denote, respectively, the left and right fixed points of $\tilde{\mathbb{W}}$ (i.e. eigenvectors associated with $\bar{\lambda}$).
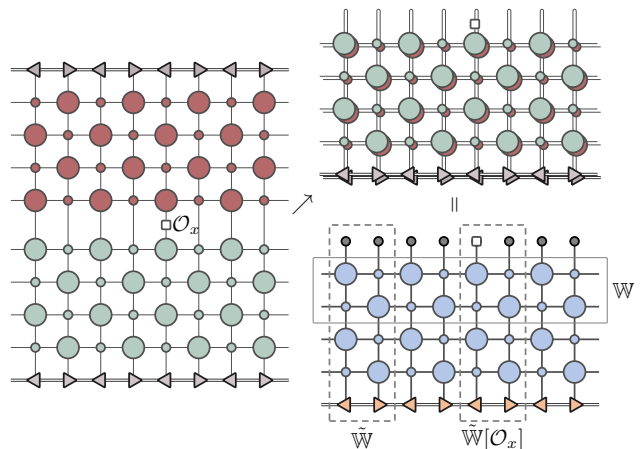

FIG. 2. Operator evolution in the MPO form starting from an MPS and the folding procedure. Time-evolution of operators can be efficiently represented by combining the tensors and their complex conjugate into a *super-tensor* acting on the doubled space.

The above reasoning can be repeated for local operators of any finite support and implies that the fixed points encode the action of the whole system on all finite subsystems, playing the role of an effective reservoir, and hence contain *all* information about local relaxation. In general, however, $\langle L|$ and $|R\rangle$ can only be obtained numerically, with a computational cost that increases exponentially with time [54, 55]. Here we show that, in Rule 54, $\langle L|$ and $|R\rangle$ can be obtained *analytically* for all times.

Before proceeding, it is important to note that $\langle L|$ and $|R\rangle$ generally bear a strong dependence on the initial state. Our goal is to identify initial MPSs that thermalize, i.e., whose local properties at large times approach those of an infinite-temperature state. One therefore expects the fixed points of $\tilde{\mathbb{W}}$ to be similar to to those of the transfer matrix $\tilde{\mathbb{W}}_\infty$, corresponding to the infinite temperature state [Note that the correlation functions on the infinite temperature state are given by the TN analogous to the one in Fig. 2, with the initial state replaced by the (appropriately normalised) identity operator]. Thus, we begin by analysing the latter.

As our first main result, we show that the fixed points of $\tilde{\mathbb{W}}_\infty$ can be computed analytically: this allows us to compute efficiently *all* infinite-temperature multi-point correlation functions supported in a finite interval, in a sense that will be made precise later [cf. Eq. (13) and subsequent discussions]. This result generalises the findings of Ref. [46] to the quantum case. Specifically, we find that the leading left and right eigenvectors can be expressed in terms of the 3×3 local tensors A_{sr}, B_{sr} and the boundary vector $|b\rangle$ (the explicit expressions are reported in the Supplemental Material)

$$
\blacklozenge\!-\!{sr} = A_{sr}, \quad \blacksquare\!-\!{sr} = B_{sr}, \quad \perp = |b\rangle,
\tag{5}
$$

that fulfil the following set of local relations, which we

term "zipping conditions"

$$
\text{(6a)}
$$

$$
\text{(6b)}
$$

Here we introduced the "classical" maximum entropy state $\overset{\circ}{\downarrow} = \begin{bmatrix} 1 & 1 & 1 & 1 \end{bmatrix}$ and the additional two-site tensor

$$
\begin{array}{c} s_1\, r_1 \\ s_2\, r_2 \end{array} = C_{s_1 r_1 s_2 r_2}. \tag{7}
$$

In terms of these local tensors, the fixed point condition for the left eigenvector has a simple diagrammatic formulation. For example for $t = 2$ we have

$$
\langle L_\infty|\,\tilde{\mathbb{W}}_\infty = \frac{1}{4}\; = \frac{1}{2}\; = \; = \langle L_\infty|. \tag{8}
$$

The prefactor $1/4$ in the diagrammatic expression of $\tilde{\mathbb{W}}_\infty$ comes from the normalisation of the infinite temperature state. To prove the fixed-point condition (8), we first apply the first relation of (6a), which replaces the bottom-most tensor A with B, and introduces the two-site tensor C in the second and third leg. The tensor C is then repeatedly moved up using the third relation in (6b), until it is absorbed at the top by applying the left-most relation in (6b). This gives the MPS with the exchanged roles of A and B. The procedure is then repeated, by using the right-most relation in (6a) and the second identity in (6b), to complete the proof of (8). The form of the right leading vector $|R_\infty\rangle$ is analogous, with the only difference that the roles of A and B are exchanged and the diagram is reflected (flipped from left to right).

Besides giving access to all infinite temperature correlations, the expressions of $\langle L_\infty|$ and $|R_\infty\rangle$ provide a natural basis to infer the structure of the fixed points $\langle L|$ and $|R\rangle$ corresponding to thermalizing initial states. Specifically, we search for fixed points taking the same form up to the boundary vector $|b\rangle$ (cf. (5)). This is because, at large times after the quench, the action of the system on its own parts has to be indistinguishable from an infinite-temperature reservoir.

To complete the ansatz, we then just have to specify a boundary vector for $\langle L|$. This is done as follows. First, given the two-site shift invariance of the problem,

we consider initial MPSs with this symmetry. Second, we observe that Eqs. (6) define a fixed point of $\tilde{\mathbb{W}}$ (with the graphical representation given in Fig. 2), provided that the following boundary identities are fulfilled

$$
\text{(9)}
$$

where $\blacktriangleleft{=}\nu = |v_\nu\rangle$, $\blacktriangleright{-}\nu = |w_\nu\rangle$, $\nu \in \{1, \ldots, \mathcal{D}\}$, are tensors to be determined. This gives

$$
\langle L|\,\tilde{\mathbb{W}} = \; = \; = \; = \langle L|. \tag{10}
$$

Eqs. (9) should be seen as a consistency equation for the bulk tensors defining the initial MPS, and the boundary vectors $|v_\nu\rangle$, $|w_\nu\rangle$. A priori, it is not obvious that a solution exists, but we find that this is indeed the case. In particular, considering the simplest case of initial product states ($\mathcal{D} = 1$), given by a pair of one-site states, $|\Psi_0\rangle = \otimes_{j=1}^{L} (|\psi_1\rangle \otimes |\psi_2\rangle)$, $\blacktriangleleft{=} = |\psi_1\rangle\,|\psi_1\rangle^*$, $\blacktriangleright{=} = |\psi_2\rangle\,|\psi_2\rangle^*$, the solution of Eq. (9) exists for the one-parameter family of states

$$
|\psi_1\rangle = \frac{1}{\sqrt{2}}\left(|0\rangle + e^{i\varphi}|1\rangle\right), \qquad |\psi_2\rangle = |0\rangle. \tag{11}
$$

The tensors $|v_1\rangle$, $|w_1\rangle$ are then uniquely determined [61]. This is our second main result: we have written the fixed points corresponding to the initial states (11) as MPSs with bond dimension three. Note that the fact that $\langle L|$ and $|R\rangle$ are not product states implies that the dynamics is not purely Markovian, in contrast to the case of dual-unitary circuits [14, 19]. Accordingly, the evolution of a given subsystem does not only depend on its state, and the quench protocol displays typical features of interacting many-body quantum systems.

In order to illustrate the power of our analytic solution, let us consider $\lim_{L\to\infty}\langle\Psi(t)|\mathcal{O}_{1;2x}|\Psi(t)\rangle$, where $\mathcal{O}_{1;2x}$ is a local operator spanning $2x$ sites. Making use of (4) and representing the r.h.s. diagrammatically (cf. (10)), we find that the expectation value can be expressed in terms of a time-independent map (matrix) $\mathcal{C}_{2x}$

$$
\langle\Psi(t)|\,\mathcal{O}_{1;2x}\,|\Psi(t)\rangle = \langle\Phi[\mathcal{O}_{1;2x}]|\,\mathcal{C}_{2x}^t\,|\Phi_{2x}\rangle, \tag{12}
$$

where the matrix $\mathcal{C}_{2x}$ and vectors $\langle\Phi[\mathcal{O}_{1;2x}]|$, $|\Phi_{2x}\rangle$ are defined graphically as

$$
\mathcal{C}_{2x} = \overbrace{\qquad\qquad}^{2x} \cdots \;, \qquad |\Phi_{2x}\rangle = \overbrace{\qquad \cdots \qquad}^{2x}, \qquad \langle\Phi[\mathcal{O}_{1;2x}]| = \underbrace{\qquad\qquad}_{2x}. \tag{13}
$$

From Eqs. (12)–(13), we see that the time evolution of operators supported on a finite number of sites can be computed either analytically or in a numerically exact fashion, by diagonalising the matrix $\mathcal{C}_{2x}$. Indeed, since the computational cost of this operation does not depend on time, once this is done the dynamics can be followed for arbitrarily large times. We note, however, that since the matrix has dimensions $9 \cdot 2^{2x}$, this procedure becomes exponentially costly as x grows. Nevertheless, Eq. (12) can always be used to show that the late-time behaviour of any operator with finite support is exponentially decaying, and to compute exactly the corresponding characteristic time τ. To see this, we use the identity
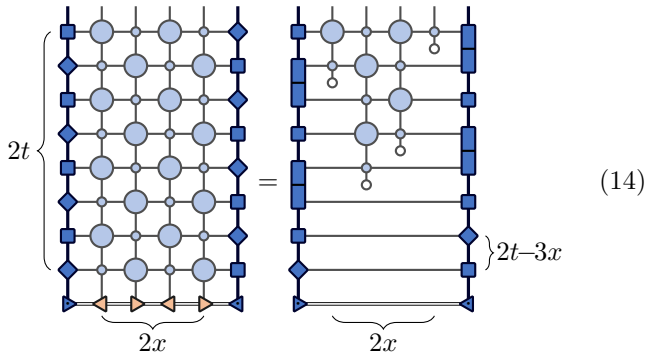
$$\qquad (14)$$

which can be proven graphically using Eqs. (6) and (9). Eq. (14) implies that for any fixed x the asymptotics of the expectation value is governed by the matrix $\mathcal{C}_0$ (cf. (13)), independent of x. It is easy to show [61] that the spectrum of $\mathcal{C}_0$ is $\{1, \lambda, \lambda^*, 0\}$, with $\lambda = (-3 + i\sqrt{7})/8$, while the only eigenvector associated with eigenvalue one is $|b\rangle \otimes |b\rangle$. This is the state that one would find at the bottom of the diagram on the l.h.s. of (14) when computing the expectation value of $\mathcal{O}_{1;2x}$ in the infinite temperature state. This means that the local observable approaches exponentially its infinite-temperature stationary value

$$\langle \Psi(t)| \, \mathcal{O}_{1:2x} \, |\Psi(t)\rangle - \mathrm{tr}[\mathcal{O}_{1;2x}\rho_{\infty,2x}] \sim \mathrm{e}^{-t/\tau} \qquad (15)$$

where $\rho_{\infty,x} = \mathbb{1}/2^x$ is the infinite temperature state on x sites and $\tau^{-1} = -2\log|\lambda| = 2\log 2$. Thus, as anticipated before, all local observables relax exponentially. This fact reflects the simple structure of our fixed points, and it is in contrast with the power-law relaxation displayed by some observables in more general integrable models [69].

Eq. (12) can also be used to study (equal-time) two-point functions of generic local observables a_x and b_y (in this case one has to choose $\mathcal{O}_{x;y} = a_x b_y$) and explicitly identify a *maximal* and a *minimal* velocity of correlation spreading. Indeed, the brickwork structure imposes a maximal speed $v_{\max} = 2$ (in our units), therefore for $t < x/2$ connected correlations are strictly zero. Additionally, Eq. (14) implies that, for $t > 3x/2$, correlations are exponentially suppressed. Namely, there exist a minimal speed $v_{\min} = 2/3$. Note that, accordingly, $v_{\min}$ and $v_{\max}$ are respectively the maximal and minimal value that the dressed velocity of quasiparticle excitations can take upon sampling all possible reference states [51].
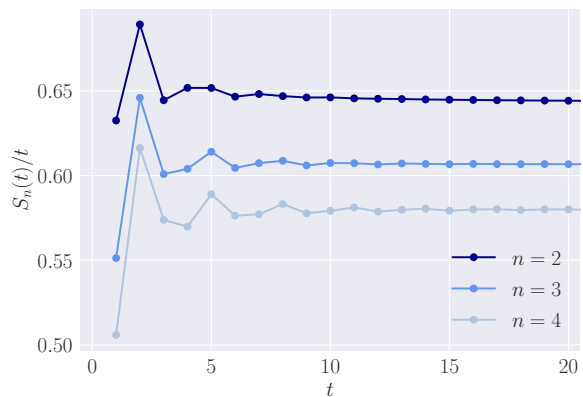

FIG. 3. Growth of Rényi entropies, for $n = 2, 3, 4$ and $\varphi = 0$. The values of $S_n(t)$ are rescaled with time.

As a last physical application, we show that our solution allows us to compute explicitly the full time evolution of the Rényi entropies after the quench. This is especially relevant in light of their accessibility in recent state-of-the-art quantum simulation experiments [70–74]. By repeating the reasoning that led to Eq. (4) in the case of $2n$ copies (or "replicas") of the time-evolution operator (n copies of $\mathbb{U}^t$ and n copies of $(\mathbb{U}^\dagger)^t$) [61] we find that $\langle L|$ and $|R\rangle$ give access to the full time evolution of the entanglement entropies of a semi-infinite interval in the thermodynamic limit [75]. This is formalised by

$$S_n(t) = \frac{\log[\mathrm{tr}[\rho_H^n(t)]]}{1 - n} = \frac{\log[\langle L|^{\otimes n} \, \mathcal{S}_{2n}(|R\rangle^*)^{\otimes n}]}{1 - n}, \quad (16)$$

where $\rho_H(t)$ is the density matrix reduced to one of the halves, $\mathcal{S}_{2n}$ is the operator performing a periodic shift by one copy in the $2n$-replica space [61], and $(\cdot)^*$ denotes complex conjugation.

Eq. (16) can again be written as the matrix element of the t-th power of a finite dimensional matrix. In particular, in this case the matrix is $3^n \times 3^n$ and we denote it by $\mathcal{T}_n$ [61]. This means that for small n we can compute $S_n(t)$ for arbitrarily large times: see, e.g., Fig. 3, where we report numerical data for $n = 2, 3, 4$. As expected for interacting integrable systems [76–80], after an initial transient, we see a clear ballistic growth with asymptotic rate given by $s_n \equiv \lim_{t\to\infty} S_n(t)/t = (\log \bar{\lambda}_n)/(1 - n)$, where $\bar{\lambda}_n$ denotes the leading eigenvalue of $\mathcal{T}_n$. Remarkably, $\bar{\lambda}_n$ can be determined exactly for arbitrary n: we find that $\bar{\lambda}_n$ is the only real solution of the equation

$$4^n x^3 - (x + 1)^2 = 0. \qquad (17)$$

The proof of this statement is non-trivial, and will be reported elsewhere [81]. To the best of our knowledge, this result provides the first exact predictions for the asymptotic growth of Rényi entropies in an interacting (non-dual-unitary) system. Furthermore, it also allows us to perform an analytic continuation and obtain predictions for arbitrary (non-integer) values of n. In particular, taking the limit $n \to 1$, we obtain the asymptotic

growth rate for the von Neumann entanglement entropy $s_1 = \log 2$. This result is particularly significant, since it represents the first exact confirmation of the quasiparticle picture for the entanglement spreading in the presence of interactions [76, 82]. Namely, it proves that the growth of von Neumann entanglement entropy can be understood in terms of pairs of correlated quasiparticles created (at each point) by the quench and moving with opposite (dressed) velocities.

In summary, in this Letter we presented an exact description of the finite-time non-equilibrium dynamics generated by a quantum quench in an interacting integrable model: the quantum cellular automaton Rule 54. The fundamental ingredient for our derivations are a set of tensor network identities, the zipping conditions (5), that enabled us to characterise exactly the action of the system on its own parts. It would be interesting to understand whether this approach can be extended to families of initial states relaxing to non-trivial GGEs, rather than to the infinite temperature state, which would enable the investigation of richer relaxation dynamics and more general dressing effects. For instance, this would provide new exact results for the spreading of entanglement, allowing us to perform a more extensive test of the quasiparticle picture for the dynamics of the von Neumann entropy and to derive analogous formulae for general Rényi entropies. Moreover, this would also enable an exact description of inhomogeneous quenches, paving the way for an ab initio derivation of Generalized Hydrodynamics [83, 84]. Another fascinating direction is to look for additional solutions of the zipping conditions. These would correspond to new exactly solvable (and possibly non-integrable) models for the discrete unitary dynamics beyond the dual-unitary case.

[1] M. Rigol, V. Dunjko, and M. Olshanii, Nature **452**, 854 (2008).

[2] M. Cazalilla and M. Rigol, New J. Phys. **12**, 055006 (2010).

[3] A. Polkovnikov, K. Sengupta, A. Silva, and M. Vengalattore, Rev. Mod. Phys. **83**, 863 (2011).

[4] L. D'Alessio, Y. Kafri, A. Polkovnikov, and M. Rigol, Adv. Phys. **65**, 239 (2016).

[5] F. H. L. Essler and M. Fagotti, J. Stat. Mech. **2016**, 064002 (2016).

[6] P. Calabrese, F. H. Essler, and G. Mussardo, J. Stat. Mech. **2016**, 064001 (2016).

[7] J.-S. Caux, J. Stat. Mech. **2016**, 064006 (2016).

[8] In fact, any continuous evolution driven by a local-Hamiltonian can be approximated arbitrarily well by a quantum circuit [85].

[9] A. Chan, A. De Luca, and J. T. Chalker, Phys. Rev. X **8**, 041019 (2018).

[10] A. Nahum, J. Ruhman, S. Vijay, and J. Haah, Phys. Rev. X **7**, 031016 (2017).

[11] A. Nahum, S. Vijay, and J. Haah, Phys. Rev. X **8**, 021014 (2018).

[12] C. W. von Keyserlingk, T. Rakovszky, F. Pollmann, and S. L. Sondhi, Phys. Rev. X **8**, 021013 (2018).

[13] B. Bertini, P. Kos, and T. Prosen, Phys. Rev. Lett. **123**, 210601 (2019).

[14] B. Bertini, P. Kos, and T. Prosen, Phys. Rev. X **9**, 021033 (2019).

[15] S. Gopalakrishnan and A. Lamacraft, Phys. Rev. B **100**, 064309 (2019).

[16] B. Bertini, P. Kos, and T. Prosen, SciPost Phys. **8**, 067 (2020).

[17] B. Bertini, P. Kos, and T. Prosen, SciPost Phys. **8**, 068 (2020).

[18] B. Bertini and L. Piroli, Phys. Rev. B **102**, 064305 (2020).

[19] L. Piroli, B. Bertini, J. I. Cirac, and T. Prosen, Phys. Rev. B **101**, 094304 (2020).

[20] P. W. Claeys and A. Lamacraft, Phys. Rev. Research **2**, 033032 (2020).

[21] B. Gutkin, P. Braun, M. Akila, D. Waltner, and T. Guhr, arXiv:2001.01298 (2020).

[22] S. A. Rather, S. Aravinda, and A. Lakshminarayan, Phys. Rev. Lett. **125**, 070501 (2020).

[23] P. Kos, B. Bertini, and T. Prosen, arXiv:2006.07304 (2020).

[24] T. Rakovszky, F. Pollmann, and C. W. von Keyserlingk, Phys. Rev. X **8**, 031058 (2018).

[25] V. Khemani, A. Vishwanath, and D. A. Huse, Phys. Rev. X **8**, 031057 (2018).

[26] A. Chan, A. De Luca, and J. T. Chalker, Phys. Rev. Lett. **121**, 060601 (2018).

[27] C. Sünderhauf, D. Pérez-García, D. A. Huse, N. Schuch, and J. I. Cirac, Phys. Rev. B **98**, 134204 (2018).

[28] A. J. Friedman, A. Chan, A. De Luca, and J. T. Chalker, Phys. Rev. Lett. **123**, 210603 (2019).

[29] Y. Li, X. Chen, and M. P. A. Fisher, Phys. Rev. B **100**, 134306 (2019).

[30] B. Skinner, J. Ruhman, and A. Nahum, Phys. Rev. X **9**, 031009 (2019).

[31] A. Zabalo, M. J. Gullans, J. H. Wilson, S. Gopalakrishnan, D. A. Huse, and J. H. Pixley, Phys. Rev. B **101**, 060301(R) (2020).

[32] Y. Bao, S. Choi, and E. Altman, Phys. Rev. B **101**, 104301 (2020).

[33] S. Choi, Y. Bao, X.-L. Qi, and E. Altman, Phys. Rev. Lett. **125**, 030505 (2020).

[34] A. Lavasani, Y. Alavirad, and M. Barkeshli, Nat. Phys. **17**, 324 (2021).

[35] P. Kos, B. Bertini, and T. Prosen, arXiv:2010.12494

[36] P. W. Claeys and A. Lamacraft, Phys. Rev. Lett. **126**, 100603 (2021).

[37] T. Rakovszky, F. Pollmann, and C. W. von Keyserlingk, Phys. Rev. Lett. **122**, 250602 (2019).

[38] A. Lerose, M. Sonner, and D. A. Abanin, arXiv:2009.10105 (2020).

[39] A. Bobenko, M. Bordemann, C. Gunn, and U. Pinkall, Commun. Math. Phys. **158**, 127 (1993).

[40] T. Prosen and C. Mejía-Monasterio, J. Phys. A: Math. Theor. **49**, 185003 (2016).

[41] S. Gopalakrishnan, Phys. Rev. B **98**, 060302(R) (2018).

[42] S. Gopalakrishnan, D. A. Huse, V. Khemani, and R. Vasseur, Phys. Rev. B **98**, 220303(R) (2018).

[43] K. Klobas, M. Medenjak, T. Prosen, and M. Vanicat, Commun. Math. Phys. **371**, 651 (2019).

[44] B. Buča, J. P. Garrahan, T. Prosen, and M. Vanicat, Phys. Rev. E **100**, 020103(R) (2019).

[45] V. Alba, J. Dubail, and M. Medenjak, Phys. Rev. Lett. **122**, 250603 (2019).

[46] K. Klobas and T. Prosen, SciPost Phys. Core **2**, 10 (2020).

[47] K. Klobas, M. Vanicat, J. P. Garrahan, and T. Prosen, J. Phys. A: Math. Theor. **53**, 335001 (2020).

[48] T. Prosen and B. Buča, J. Phys. A: Math. Theor. **50**, 395002 (2017).

[49] A. Inoue and S. Takesue, J. Phys. A: Math. Theor. **51**, 425001 (2018).

[50] V. Alba, arXiv:2006.02788 (2020).

[51] A. J. Friedman, S. Gopalakrishnan, and R. Vasseur, Phys. Rev. Lett. **123**, 170603 (2019).

[52] L. E. Hillberry, M. T. Jones, D. L. Vargas, P. Rall, N. Y. Halpern, N. Bao, S. Notarnicola, S. Montangero, and L. D. Carr, arXiv:2005.01763 (2020).

[53] S. Gopalakrishnan and B. Zakirov, Quantum Science Tech. **3**, 044004 (2018).

[54] M. C. Bañuls, M. B. Hastings, F. Verstraete, and J. I. Cirac, Phys. Rev. Lett. **102**, 240603 (2009).

[55] A. Müller-Hermes, J. I. Cirac, and M. C. Bañuls, New J. Phys. **14**, 075003 (2012).

[56] M. B. Hastings and R. Mahajan, Phys. Rev. A **91**, 032306 (2015).

[57] P. Calabrese and J. Cardy, Phys. Rev. Lett. **96**, 136801 (2006).

[58] P. Calabrese and J. Cardy, J. Stat. Mech. **2007**, P06008 (2007).

[59] M. Fannes, B. Nachtergaele, and R. F. Werner, Commun. Math. Phys. **144**, 443 (1992).

[60] D. Perez-Garcia, F. Verstraete, M. Wolf, and J. Cirac, Quant. Inf. Comput. **7**, 401 (2007).

[61] See the Supplemental Material.

[62] J. I. Cirac, D. Perez-Garcia, N. Schuch, and F. Verstraete, J. Stat. Mech. **2017**, 083105 (2017).

[63] M. B. Sahinoglu, S. K. Shukla, F. Bi, and X. Chen, Phys. Rev. B **98**, 245122 (2018).

[64] L. Piroli and J. I. Cirac, Phys. Rev. Lett. **125**, 190402 (2020).

[65] B. Bertini, P. Kos, and T. Prosen, Phys. Rev. Lett. **121**, 264101 (2018).

[66] A. Flack, B. Bertini, and T. Prosen, Phys. Rev. Research **2**, 043403 (2020).

[67] P. Braun, D. Waltner, M. Akila, B. Gutkin, and T. Guhr, Phys. Rev. E **101**, 052201 (2020).

[68] S. J. Garratt and J. Chalker, arXiv:2008.01697 (2020).

[69] J. De Nardis, L. Piroli, and J.-S. Caux, J. Phys. A: Math. Theor. **48**, 43FT01 (2015).

[70] R. Islam, R. Ma, P. M. Preiss, M. E. Tai, A. Lukin, M. Rispoli, and M. Greiner, Nature **528**, 77 (2015).

[71] A. M. Kaufman, M. E. Tai, A. Lukin, M. Rispoli, R. Schittko, P. M. Preiss, and M. Greiner, Science **353**, 794 (2016).

[72] N. M. Linke, S. Johri, C. Figgatt, K. A. Landsman, A. Y. Matsuura, and C. Monroe, Phys. Rev. A **98**, 052334 (2018).

[73] A. Lukin, M. Rispoli, R. Schittko, M. E. Tai, A. M. Kaufman, S. Choi, V. Khemani, J. Léonard, and M. Greiner, Science **364**, 256 (2019).

[74] A. Elben, R. Kueng, H. Y. R. Huang, R. van Bijnen, C. Kokail, M. Dalmonte, P. Calabrese, B. Kraus, J. Preskill, P. Zoller, and B. Vermersch, Phys. Rev. Lett. **125**, 200501 (2020).

[75] Here, for simplicity, we consider open boundary conditions.

[76] V. Alba and P. Calabrese, PNAS **114**, 7947 (2017).

[77] V. Alba and P. Calabrese, SciPost Phys. **4**, 17 (2018).

[78] V. Alba and P. Calabrese, Phys. Rev. B **96**, 115421 (2017).

[79] V. Alba and P. Calabrese, J. Stat. Mech. **2017**, 113105 (2017).

[80] M. Mestyán, V. Alba, and P. Calabrese, J. Stat. Mech. **2018**, 083104 (2018).

[81] K. Klobas, B. Bertini, and L. Piroli, in preparation.

[82] In Rule 54 quasiparticles have no dispersion, the infinite-temperature dressed velocity is 1 [42] and the Yang-Yang entropy of the infinite temperature state is $\log 2$. Replacing these definitions in the prediction of Ref. [76] gives us $s_1 = \log 2$.

[83] O. A. Castro-Alvaredo, B. Doyon, and T. Yoshimura, Phys. Rev. X **6**, 041065 (2016).

[84] B. Bertini, M. Collura, J. De Nardis, and M. Fagotti, Phys. Rev. Lett. **117**, 207201 (2016).

[85] T. J. Osborne, Phys. Rev. Lett. **97**, 157202 (2006).

Supplemental Material for
Exact Thermalization Dynamics in the "Rule 54" Quantum Cellular Automaton

Here we report some useful information complementing the main text. In particular

- In Section A we derive the tensor-network representation of Rule 54;

- In Section B we study the spectrum of the transfer matrix in space;

- In Section C we provide the explicit form of matrices and boundary vectors defining the MPS representation of the fixed points

- In Section D we report the matrix elements of $\mathcal{C}_0$.

- In Section E we provide additional detail on the calculation of Rényi entropies.

Appendix A: Tensor network representation of Rule 54

Time evolution in the model is obtained by consecutive application of the three-site local unitary gate U given by (1). Defining the following two tensors,

$$
\begin{array}{c}
\substack{s_4 \\ \\ s_1 \!-\!\!\bigcirc\!\!-\! s_3 \\ \\ s_2}
\end{array} = \delta_{\chi(s_1,s_2,s_3),s_4}, \qquad
s_1 \!-\!\!\underset{s_2 \quad s_3}{\overset{\ddots}{\bullet}}^{s_k} = \prod_{j=1}^{k-1} \delta_{s_j,s_{j+1}},
\tag{A1}
$$

one realizes that the three-site operator can be equivalently expressed as

$$
U = \boxed{} = \bullet\!\!-\!\!\bigcirc\!\!-\!\!\bullet.
\tag{A2}
$$

The equivalence between the two sides in Fig. 1 then follows from a simple identity satisfied by the second tensor,

$$
\tag{A3}
$$

Appendix B: Spectrum of the transverse transfer matrix

The unitarity of time-evolution implies

$$
1 = \langle \Psi(t)|\Psi(t) \rangle = \mathrm{tr}\left(\tilde{\mathbb{W}}^L \right) = \sum_j \lambda_j^L,
\tag{B1}
$$

where the second equality follows directly from the definition of the transverse transfer matrix (3) and λ_j are eigenvalues of $\tilde{\mathbb{W}}$. This equality holds for any L, which means that $\lambda_j \in \{0,1\}$ and both the geometric and algebraic multiplicity of the eigenvalue 1 has to be 1.

Appendix C: MPS representation of the leading eigenvectors

Here we report an explicit representation for the 3×3 matrices A_{sr}, B_{sr}, and $C_{s_1 r_1 s_2 r_2}$ fulfilling relations (6a)–(6b) and (9). The non identically vanishing matrices in the set are given by

$$A_{00} = \frac{1}{2} \begin{bmatrix} 1 & 1 & -1 \\ 1 & 1 & 1 \\ 1 & -1 & -1 \end{bmatrix}, \qquad A_{01} = A_{10} = \frac{1}{2} \begin{bmatrix} 0 & 1 & -1 \\ 1 & 0 & 0 \\ 1 & 0 & 0 \end{bmatrix}, \qquad A_{11} = \begin{bmatrix} 0 & 1 & 0 \\ 1 & 0 & 0 \\ 0 & 0 & 0 \end{bmatrix},$$

$$B_{00} = \begin{bmatrix} 1 & 0 & 0 \\ 0 & 0 & 0 \\ 0 & 0 & 0 \end{bmatrix}, \qquad B_{11} = \begin{bmatrix} 0 & 0 & 0 \\ 0 & 1 & 0 \\ 0 & 0 & 1 \end{bmatrix},$$

$$C_{0001} = C_{0010} = \frac{1}{4} \begin{bmatrix} 0 & 1 & -1 \\ 0 & 1 & -1 \\ 0 & -1 & 1 \end{bmatrix}, \quad C_{0101} = C_{1010} = \frac{1}{4} \begin{bmatrix} 0 & 0 & 0 \\ 1 & 0 & 0 \\ 1 & 0 & 0 \end{bmatrix}, \quad C_{0110} = C_{1001} = \frac{1}{4} \begin{bmatrix} 0 & 0 & 0 \\ 0 & 1 & 1 \\ 0 & 1 & 1 \end{bmatrix}, \qquad \text{(C1)}$$

$$C_{1101} = C_{1110} = \frac{1}{2} \begin{bmatrix} 1 & 0 & 0 \\ 0 & 0 & 0 \\ 0 & 0 & 0 \end{bmatrix}, \qquad C_{0000} = \frac{1}{4} \begin{bmatrix} 1 & 1 & -1 \\ 1 & 1 & -1 \\ 1 & -1 & 1 \end{bmatrix}, \qquad C_{0011} = \frac{1}{2} \begin{bmatrix} 0 & 1 & 0 \\ 0 & 1 & 0 \\ 0 & 0 & 1 \end{bmatrix},$$

$$C_{1100} = \frac{1}{2} \begin{bmatrix} 1 & 0 & 0 \\ 0 & 1 & 1 \\ 0 & 0 & 0 \end{bmatrix}, \qquad C_{1111} = \frac{1}{2} \begin{bmatrix} 1 & 0 & 0 \\ 1 & 0 & 0 \\ 0 & 0 & 0 \end{bmatrix},$$

while the appropriate boundary vectors $|b\rangle$, $|v_1\rangle$, $|w_1\rangle$ are

$$|b\rangle = \frac{1}{\sqrt{2}} \begin{bmatrix} 1 \\ 1 \\ 0 \end{bmatrix}, \qquad |v_1\rangle = \frac{1}{\sqrt{2}} \begin{bmatrix} 1 \\ 1 \\ -1 \end{bmatrix}, \qquad |w_1\rangle = \sqrt{2} \begin{bmatrix} 1 \\ 0 \\ 0 \end{bmatrix}. \qquad \text{(C2)}$$

Note that this choice of magnitude of boundary vectors implies the normalisation of leading eigenvectors of the transverse transfer matrix

$$\langle L_\infty | R_\infty \rangle = \langle b | b \rangle^2 = 1, \qquad \langle L | R \rangle = \langle b | v \rangle \langle b | w \rangle = 1. \qquad \text{(C3)}$$

The latter equations follow from Eq. (13) and $\langle b | \otimes \langle b | \, \mathcal{C}_0 = \langle b | \otimes \langle b |$.

Appendix D: Spectrum of the matrix $\mathcal{C}_0$

By definition (13), the matrix $\mathcal{C}_0$ can be expressed as

$$\mathcal{C}_0 = \quad = \frac{1}{4} \begin{bmatrix} 1 & 0 & 0 & 1 & 2 & -2 & -1 & 0 & 0 \\ 1 & 0 & 0 & 1 & 2 & 2 & -1 & 0 & 0 \\ 1 & 0 & 0 & 1 & -2 & -2 & -1 & 0 & 0 \\ 0 & 4 & 0 & 0 & 0 & 0 & 0 & 0 & 0 \\ 2 & 0 & 0 & 2 & 0 & 0 & 2 & 0 & 0 \\ 0 & 0 & 0 & 0 & 0 & 0 & 0 & 0 & 0 \\ 0 & 0 & 0 & 0 & 0 & 0 & 0 & 0 & 0 \\ 2 & 0 & 0 & -2 & 0 & 0 & -2 & 0 & 0 \\ 0 & 0 & 0 & 0 & 0 & 0 & 0 & 0 & 0 \end{bmatrix}. \qquad \text{(D1)}$$

It is easy to verify that it has 3 non-zero eigenvalues with geometric and algebraic multiplicities equal to 1. Explicitly

$$\text{Sp}\,(\mathcal{C}_0) = \left\{ 1, -\frac{3}{8} + \mathrm{i} \frac{\sqrt{7}}{8}, -\frac{3}{8} - \mathrm{i} \frac{\sqrt{7}}{8}, 0 \right\}. \qquad \text{(D2)}$$

Appendix E: Tensor network formulation of Rényi entanglement entropies

We start by considering the density matrix at time t (at time 0 the system has been initialised in an MPS fulfilling (9)) reduced to one of the halves

$$\rho_H(t) = \frac{1}{\mathcal{N}_L} \quad \vcenter{\hbox{}} . \tag{E1}$$

Here we took *open* boundary conditions and introduced the constant $\mathcal{N}_L$ to ensure $\mathrm{tr}[\rho_H(t)] = 1$. Note that $\lim_{L\to\infty} \mathcal{N}_L = (\langle B_L| \otimes \langle B_L|^*) |R\rangle \langle L| (|B_R\rangle \otimes |B_R\rangle^*)$ where $\langle B_L|, |B_R\rangle \in \mathbb{C}^{2^{2t}}$ are the vectors in the t-direction encoding the (left and right) boundary conditions, the tensor product acts on different copies, and $(\cdot)^*$ denotes complex conjugation. Note that $\langle B_L|$ and $|B_R\rangle$ are defined in one copy of the time-sheet, while $\langle L|, |R\rangle \in \mathbb{C}^{2^{4t}}$ live in the tensor product of two copies.

Considering now the trace of, e.g., the third power of the reduced density matrix we have

$$\mathrm{tr}[\rho_H^3(t)] = \frac{1}{\mathcal{N}_L^3} \quad \vcenter{\hbox{}} , \tag{E2}$$

where green and red areas represent the TNs associated with U and $U^\dagger$ respectively, cf. Eq. (E1). Using the t-channel language of Eq. (3), we see that this object can be written as

$$\mathrm{tr}[\rho_H^3(t)] = \frac{1}{\mathcal{N}_L^3} (\langle B_L| \otimes \langle B_L|^*)^{\otimes 3} (\tilde{\mathbb{W}}^{\otimes 3})^L \mathcal{S}_6 ((\tilde{\mathbb{W}}^*)^{\otimes 3})^L (|B_R\rangle^* \otimes |B_R\rangle), \tag{E3}$$

where $\mathcal{S}_6$ is the periodic shift by one in the space of the 6 replicas. Namely it acts on the Hilbert space

$$\mathcal{H}_6 = \left(\mathbb{C}^{2^{2t}}\right)^{\otimes 6} \tag{E4}$$

as follows

$$\mathcal{S}_6 |i_1\rangle \otimes |i_2\rangle \otimes |i_3\rangle \otimes |i_4\rangle \otimes |i_5\rangle \otimes |i_6\rangle = |i_2\rangle \otimes |i_3\rangle \otimes |i_4\rangle \otimes |i_5\rangle \otimes |i_6\rangle \otimes |i_1\rangle , \qquad i_j = 0, 1, \dots 2^{2t} - 1, \tag{E5}$$

where $\{|i\rangle\}_{i=0}^{2^{2t}-1}$ is a basis of $\mathbb{C}^{2^{2t}}$.

In the thermodynamic limit we can make the replacement

$$\tilde{\mathbb{W}} \mapsto |R\rangle\langle L| , \qquad \tilde{\mathbb{W}}^* \mapsto |R\rangle^*\langle L|^* , \qquad \mathcal{N}_L \mapsto (\langle B_L| \otimes \langle B_L|^*) |R\rangle \langle L| (|B_R\rangle \otimes |B_R\rangle^*), \tag{E6}$$

and use

$$(\langle B_L| \otimes \langle B_L|^*) |R\rangle = (\langle B_L|^* \otimes \langle B_L|) |R\rangle^* , \qquad \langle L| (|B_R\rangle \otimes |B_R\rangle^*) = \langle L|^* (|B_R\rangle^* \otimes |B_R\rangle), \tag{E7}$$

to find

$$\lim_{L\to\infty} \mathrm{tr}[\rho_H^3(t)] = \langle L|^{\otimes 3}\, \mathcal{S}_6(|R\rangle^*)^{\otimes 3}\,. \tag{E8}$$

An analogous reasoning considering a generic n-th power leads to (16). Note that for periodic boundary conditions the r.h.s. of (E8) is replaced by its square.

Finally, we note that (E8) can be represented in terms of the matrix element of the t-th power of a time-independent matrix. Indeed, "unfolding" the tensors (5), i.e.

$$\tag{E9}$$

we have

$$\langle L|^{\otimes 3}\, \mathcal{S}_6(|R\rangle^*)^{\otimes 3} = \langle \mathcal{U}_3|\, \mathcal{T}_3^t\, |\mathcal{D}_3\rangle\,, \tag{E10}$$

with

$$\tag{E11}$$